Electrical transport and optical properties of the incommensurate intergrowth compounds $(SbS)_{1.15}(TiS_2)_n$ with $n = 1$ and 2

2002 J. Phys.: Condens. Matter 14 8011

(http://iopscience.iop.org/0953-8984/14/34/320)

INSTITUTE OF PHYSICS PUBLISHING JOURNAL OF PHYSICS: CONDENSED MATTER

J. Phys.: Condens. Matter **14** (2002) 8011–8023 PII: S0953-8984(02)35010-0

Electrical transport and optical properties of the incommensurate intergrowth compounds $(SbS)_{1.15}(TiS_2)_n$ with $n = 1$ and 2

Y Ren[1,3], C H Rüscher[2], C Haas[1] and G A Wiegers[1]

[1] Chemical Physics, Materials Science Centre, University of Groningen, Nijenborgh 4, 9747 AG Groningen, The Netherlands
[2] Institut für Mineralogie der Universität Hannover, Welfengarten 1, D-30167 Hannover, Germany

Received 18 March 2002
Published 15 August 2002
Online at stacks.iop.org/JPhysCM/14/8011

Abstract

The in-plane electrical transport and optical properties of the incommensurate intergrowth compounds $(SbS)_{1.15}(TiS_2)_n$ with $n = 1, 2$ have been investigated by means of measurements of the electrical resistivity, Hall coefficient and thermopower in the temperature range from 4.2 to 350 K, and by optical spectroscopy in the frequency range 1000–20 000 cm^{-1} at room temperature. Both the Hall effect and the thermopower indicate transport by electrons. The Hall coefficients show electron donation of about 0.57 and 0.34 of an electron per Ti atom for $(SbS)_{1.15}(TiS_2)_n$ with $n = 1$ and 2, respectively. The in-plane resistivity $\rho_{ab}(T)$ exhibits a non-linear dependence on temperature, which can be described with the formula $\rho_{ab}(T) = \rho_0 + A_{ee}(T/T_F)^2 \ln(T_F/T)$ as for a two-dimensional Fermi liquid. Fits according to the Drude model to the room temperature optical reflectivity show that the relaxation rate has a quadratic variation with frequency $1/\tau(\omega) \sim \omega^2$, also indicating Fermi-liquid behaviour with interelectronic collisions of quasiparticles. Only a small anisotropy in the ab-plane is observed in the optical spectra for the electrical field polarized parallel and perpendicular to the incommensurate direction.

1. Introduction

The so-called misfit layer compounds, denoted by $(\mathcal{MX})_{1+\delta}(\mathcal{TX}_2)_n$ ($\mathcal{M}$ = Sn, Pb, Bi, Sb, rare-earth elements; $\mathcal{T}$ = Ti, V, Cr, Nb, Ta; $\mathcal{X}$ = S, Se; and $n = 1, 2, 3$), form the class of intergrowth structures [1, 2]. They are built up by an alternate stacking of $\mathcal{MX}$ double layers with a distorted rock-salt structure and $(\mathcal{TX}_2)_n$ sandwiches with $\mathcal{T}$ in trigonal or anti-trigonal prisms of $\mathcal{X}$ depending on the transition metal $\mathcal{T}$. The crystal structures are characterized by the two mutually modulated subsystems, which can be described with *superspace groups* [3], and δ is defined by the volume ratio of the unit cells of two subsystems.

[3] Present address: Argonne National Laboratory, 9700 S. Cass Avenue, Argonne, IL 60439, USA.

The physical properties of the misfit layer compounds, like the electrical transport and optical reflectivity, are closely related to the $\mathcal{TX}_2$ part of the compounds (see [1, 4, 5] and references therein). According to this the misfit layer compounds may be considered to be similar to intercalates of transition metal dichalcogenides, $\mathcal{M}'_x\mathcal{TX}_2$ ($\mathcal{M}'$ = alkali metals, Ib metals, transition metals). These compounds have been the subject of many investigations [6–9]. Among them 1T-TiS_2 has evoked much controversy regarding whether it is a semimetal or a doped semiconductor (see [10, 11] and references therein). 1T-TiS_2 and its intercalates exhibit an anomalous temperature dependence on the electrical resistivity, which can be expressed in the form of a simple power law $\rho = \rho_0 + AT^\alpha$ with an exponent α around 2 [12]. The deviation from the ideal $\rho \approx T^2$ for stoichiometric TiS_2 indicates that the conduction mechanism cannot be interpreted simply in terms of electron–electron scattering in a 3D Fermi-liquid system. Klipstein *et al* [13] have explained this anomaly by an unusual phonon scattering mechanism. Taking into account the electron valleys at the L and M points of the Brillouin zone (BZ) of 1T-TiS_2, these authors have shown that a model involving both intravalley and intervalley scattering by acoustic phonons can account for the temperature dependence of the resistivity of TiS_2. Koyano *et al* [8] were able to explain the temperature dependence of the electrical resistivity and thermopower of TiS_2 and its intercalates $\mathcal{M}'TiS_2$ ($\mathcal{M}'$ = Mn, Fe, Co and Ni) using a single-carrier picture with a scattering mechanism based on the idea of Klipstein *et al* [13]. It may be noted that Julien *et al* [14] have found that the optical reflectivity of 1T-TiS_2 provides evidence for the dominance of electron–electron scattering in the Drude relaxation with a frequency variation expected for a Fermi liquid.

In first studies on the electrical properties of the misfit layer compounds $(SnS)_{1.20}TiS_2$ and $(PbS)_{1.18}TiS_2$, it was found that the resistivity also follows power-law behaviour ($\alpha \approx 1.5$) [15], similarly to the properties of the pristine TiS_2. Therefore, it is interesting to investigate the properties of Ti-based misfit layer compounds in further detail. The concern of this study are the compounds $(SbS)_{1.15}(TiS_2)_n$ with $n = 1, 2$.

The complete crystal structures of the Sb-containing misfit layer compounds, $(SbS)_{1.15}(TiS_2)_n$ with $n = 1$ and 2, have been described in terms of a (3 + 2)-dimensional superspace group [16, 17]. They can be considered as SbS intercalation compounds of TiS_2 with a stage-1 and a stage-2 structure for $n = 1$ and 2, respectively. (In $(SbS)_{1.15}TiS_2$ the two subsystems SbS and TiS_2 stack alternately, whereas the stage-2 compound $(SbS)_{1.15}(TiS_2)_2$ consists of paired sandwiches TiS_2 with a stacking sequence $\cdots$ [TiS_2][SbS][TiS_2][TiS_2][SbS][TiS_2] $\cdots$.) The structures projected along the common [100] direction are depicted in figures 1(a) and (b) for $n = 1$ and 2 respectively. Both subsystems TiS_2 and SbS have triclinic symmetry. The lattice parameters of the two subsystems are given in table 1. The Ti atoms are surrounded by six S atoms in a slightly distorted octahedral coordination. Besides the mutual modulation between the SbS and TiS_2 subsystems, an extra modulation with a wavevector $\vec{q} = 0.818(\vec{a}^*_{SbS} + \vec{b}^*_{SbS})$ along the [110] diagonal of the SbS reciprocal lattice indicates an ordering of the Sb/S atoms on the rock-salt structure. The structure determination revealed zigzag clusters of Sb–Sb and S–S contacts along the [$1\bar{1}0$] direction of the SbS lattice. Statistically, 22% of the Sb atoms are in Sb–Sb bonds, which has been confirmed by x-ray photoelectron spectroscopy [18]. Figure 1(c) shows the interface-modulated ordering of Sb/S in the SbS subsystem in a supercell approximation, (occupancy larger than 0.6), while the zigzag chains of open circles are mainly of S atoms.

In this paper we present results on the electrical transport and optical properties of $(SbS)_{1.15}(TiS_3)_n$ with $n = 1, 2$, obtained using resistivity, Hall coefficient and thermopower measurements as well as reflection and transmission spectroscopy of very thin specimens. Polarized optical reflectivity measurements were performed in order to investigate the anisotropy within the *ab*-plane of the crystals. The experimental data are analysed using different models.

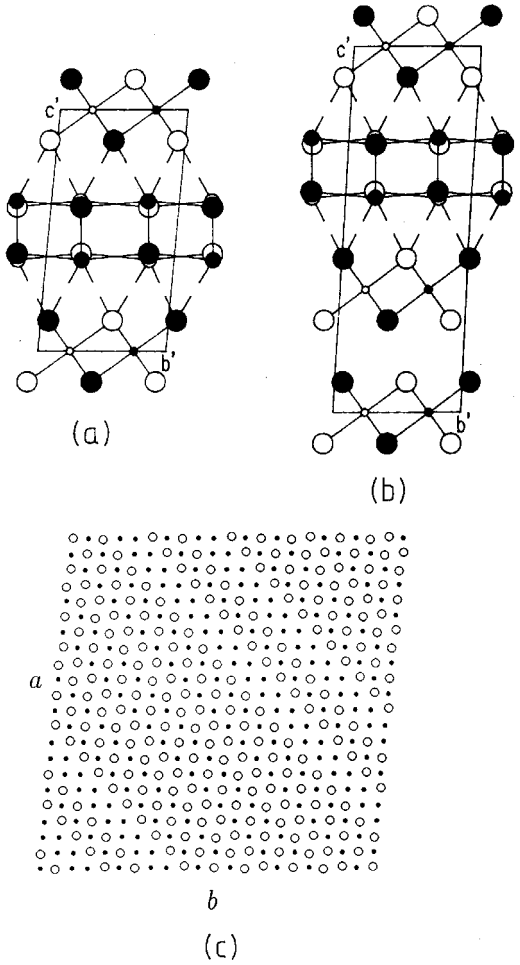

Figure 1. Orthogonal projection of the structure of $(SbS)_{1.15}(TiS_2)_n$ along the common [100] direction (a) for $n = 1$ and (b) for $n = 2$. $b' = a_{\nu 2}\sin\gamma_\nu$ and $c' = a_{\nu 3}\sin\beta_\nu$ for $\nu = 1, 2$. Large open and filled circles denote S atoms, small open and filled circles denote Ti atoms and circles of intermediate size denote Sb atoms. (c) One layer of the *ab*-planes of the modulated structure of the SbS subsystem. Small filled circles are Sb atoms and large open circles are S atoms. In the antiphase boundaries only Sb–Sb and S–S clusters exist, instead of the continuous chains as shown here for clarity.

Table 1. Subsystem unit-cell dimensions of $(SbS)_{1.15}TiS_2$ and $(SbS)_{1.15}(TiS_2)_2$.

Compound	Subsystem	ν	$a_{\nu 1}$ (Å)	$a_{\nu 2}$ (Å)	$a_{\nu 3}$ (Å)	α_ν (deg)	β_ν (deg)	γ_ν (deg)
$(SbS)_{1.15}TiS_2$	TiS_2	1	3.403(1)	5.911(1)	11.385(1)	84.39(1)	82.817(8)	90.01(1)
	SbS	2	5.908(2)	5.936(2)	11.311(1)	83.973(8)	85.87(1)	84.06(1)
$(SbS)_{1.15}(TiS_2)_2$	TiS_2	1	3.405(4)	5.898(4)	17.030(2)	86.39(2)	84.94(2)	89.96(2)
	SbS	2	5.902(4)	5.924(4)	17.019(2)	85.93(2)	85.38(2)	84.23(2)

2. Experimental details

Compounds $(SbS)_{1+\delta}TiS_2$ and $(SbS)_{1+\delta}(TiS_2)_2$ were synthesized from the elements by high-temperature reaction. The mixtures of elements Sb, Ti and S, in the ratio with $\delta = 0.12$, were

sealed in evacuated quartz ampoules and heated in a single-zone furnace at 300 °C for two days and at 450 °C for one day. The ampoules were then kept at 620 °C for one month during which single crystals were formed. Single crystals of dimensions up to $2 \times 2 \times 0.02$ mm^3 are thin platelets with a silver lustre. The crystals were characterized by x-ray techniques. In-plane electrical resistivities (ρ_{ab}) and Hall coefficients (R_H) (the magnetic field applied along the c-axis) were measured in the temperature range 4.2–350 K using the four- and five-point-contact methods on single-crystal platelets with a rectangular shape. Contacts were made on the edges using silver paste. Thermopower (S) measurements were performed on powder compacts of the compounds in the temperature range 4.2–300 K using a microcomputer for control of the temperature and temperature gradient and the measurement of the thermo-EMF; the thermopower was determined by a least-squares fit to the EMF versus gradient data.

The same crystals of the misfit layer compounds as were used for the resistivity and Hall effect measurements were also used for the optical reflectivity measurements. The crystals were glued with their flat side to the sample holders. The surfaces were cleaned by stripping away several layers. The reflection spectra were measured in the frequency range 600–20 000 cm^{-1} using a Fourier transform infrared (FTIR) spectrometer equipped with an infrared microscope (*Bruker IFS88, A590*) and with Au-grid (*KRS5*) and prism polarizers (*Glan Thompson K*) for the incident light. The use of a microscope enables us to focus the incident light on very small spots ($<$90 μm) of the sample surfaces. This made it possible to measure the transmission spectra of very thin films. The absolute value of the reflectivity was obtained using uncoated Ag and Al mirrors together with a $SrTiO_3$ standard sample. The absolute accuracy of the reflectivity data is about 5%; the relative accuracy is better than 0.5%.

3. Electrical transport properties

The temperature dependences of the in-plane electrical resistivities ρ_{ab} for the two misfit layer compounds are shown in figure 2. Experimental results on the electrical transport properties are listed in table 2. The residual resistivity ratio (RRR), which is defined as the ratio of the resistivity at room temperature to the residual resistivity at $T = 0$ K, $\rho_{RT}/\rho_0 = 4.0$ for $(SbS)_{1.15}(TiS_2)_2$ and 7.4 for $(SbS)_{1.15}TiS_2$. The smaller value for the stage-2 misfit layer compound may be due to an ionized impurity scattering caused by self-intercalated Ti atoms in the empty van der Waals gaps. The variation of the in-plane resistivity with temperature over the range 100–350 K can be described with an expression of the form $\rho = \rho_0 + AT^\alpha$. The least-squares fitting procedure indicates the exponent to be $\alpha = 1.41 \pm 0.02$ for $(SbS)_{1.15}TiS_2$ and $\alpha = 1.32 \pm 0.02$ for $(SbS)_{1.15}(TiS_2)_2$, close to the values for the intercalates Li_xTiS_2 [19] and $Ag_{0.33}TiS_2$ [20] and other TiS_2-based misfit layer compounds [2], but smaller than that for pure 1T-TiS_2 ($\alpha \approx 2.2$) [13]. This temperature dependence is stronger than expected for acoustic phonon scattering in simple metals ($\alpha = 1$), but weaker than that for electron–electron scattering in a 3D Fermi-liquid system ($\alpha = 2$) which was used by Thompson [21] to interpret the temperature dependence of the in-plane resistivity of high-purity, stoichiometric 1T-TiS_2.

According to a detailed analysis given by Klipstein *et al* [13], both optical and acoustic phonons contribute to the resistivity in TiS_2: optical phonons account for the temperature dependence of the resistivity above room temperature, while longitudinal acoustic (LA) phonons provide the dominant contribution to the electron scattering below room temperature. Furthermore, taking into account the electron valleys at the L and M points of the BZ of 1T-TiS_2, they have shown that a model involving both intravalley and intervalley scattering by acoustic phonons can account for the temperature dependence of the resistivity of TiS_2. On the basis of this model, Koyano *et al* [8] have analysed the temperature dependence of the electrical resistivity and thermopower of TiS_2 and its intercalates $\mathcal{M}'_xTiS_2$ ($\mathcal{M}'$ = Mn, Fe,

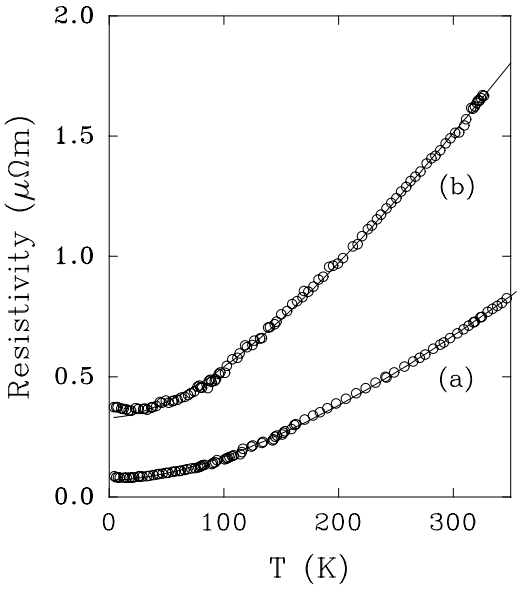

Figure 2. The temperature dependence of the in-plane resistivity ρ_{ab} of (a) $(SbS)_{1.15}TiS_2$ and (b) $(SbS)_{1.15}(TiS_2)_2$. The open circles show measured data and the solid curves are curves calculated using the 2D Fermi-liquid model (equation (1)).

Table 2. Experimental results on the resistivity ρ_{ab} (units of 10^{-8} Ω m), $RRR_{ab} = \rho_{ab}(RT)\rho_{ab}(0)$, Hall coefficient R_H (units of 10^{-9} m^3 C^{-1}), electron concentration n_e (units of 10^{27} m^{-3}), occupancy y of the Ti 3d conduction band and thermoelectric power S (units of μV K^{-1}) for $(SbS)_{1.15}(TiS_2)_n$ ($n = 1, 2$).

	ρ_{ab}			$R_H(n_e)$		y	S
Compound	4.2 K	RT	RRR_{ab}	4.2 K	RT	4.2 K	RT
$(SbS)_{1.15}TiS_2$	8.9	66	7.4	−1.24 (5.0)	−1.08 (5.8)	0.57	−25.5
$(SbS)_{1.15}(TiS_2)_2$	37	148	4.0	−1.56 (4.0)	−1.84 (3.4)	0.34	−32.4

Co and Ni) using a single-carrier model. Attempts to use this model to analyse the resistivity data of the misfit layer compounds $(SbS)_{1.15}(TiS_2)_n$ with $n = 1, 2$ did not give reasonable parameters.

For 1T-Ti_xS_2 [13] and its intercalates Li_xTiS_2 [19], it has been found that the exponent α in the power-law expression decreases with increasing carrier concentration as expected in the model of Klipstein *et al* [13]. In the present misfit layer compounds, however, one finds that the exponent α increases with increasing carrier concentration. This behaviour is similar to that observed for some high-T_c superconducting oxides. The system $La_{2-x}Sr_xCuO_4$ shows in the overdoped range ($x > 0.2$) a power-law dependence of the in-plane resistivity ρ_{ab} of the normal state: $\rho_{ab} \propto T^{\alpha}$ with $\alpha = 1.5$ [22]. For $Pr_{2-x}Ce_xCuO_{4-\delta}$ the exponent α increases with increasing Ce concentration, i.e. with increasing electron doping of the CuO_2 planes [23]. Using this, the non-linear temperature dependence of the normal-state resistivity in such superconductors has been explained in terms of electron–electron interactions in these layered structures [24]. Following this line of argument, theoretical calculations may be considered. For this case, the electrical resistivity of a two-dimensional Fermi-liquid system

Table 3. The values of ρ_0, A_{ee} and T_F in equation (7) as obtained from the fits to the in-plane resistivity of the misfit layer compounds. The Fermi energies E_F are derived from the definition $E_F = k_B T_F$.

Compound	ρ_0 ($\mu\Omega$ m)	A_{ee} ($\mu\Omega$ m K^{-2})	T_F (10^3 K)	E_F (eV)
$(SbS)_{1.15}TiS_2$	0.070(1)	32(4)	3.4(3)	0.29(3)
$(SbS)_{1.15}(TiS_2)_2$	0.333(3)	25(2)	1.8(1)	0.16(1)

can be expressed as [25, 26]

$$\rho(T) = \rho_0 + A_{ee}\left(\frac{T}{T_F}\right)^2 \ln\frac{T_F}{T}, \tag{1}$$

where ρ_0 is the temperature-independent residual resistivity, A_{ee} a constant and T_F the Fermi temperature. Using equation (1), the temperature-dependent variations of the in-plane resistivity for the two misfit layer compounds were re-analysed. The fits to the resistivities for the entire temperature range from 4.2 to 350 K show a very good agreement between the theory and the experimental data (figure 2). The fit parameters (ρ_0, A_{ee} and T_F) are listed in table 3. It can be seen from equation (1) that T_F and, related to this, the Fermi energy $E_F = k_B T_F$ depend only on the variation of $\rho(T)$ on the temperature, and are independent of the uncertainty in the measurement of the thickness of the thin crystals and thus the absolute values of the resistivity. Therefore, the Fermi energy can be obtained rather accurately within this model. It is observed that the Fermi level of the stage-1 compound is 0.13 eV higher than that of the stage-2 compound, corresponding to a higher electron filling in the Ti 3d conduction band. This observation is in agreement with results on soft x-ray absorption spectroscopy (XAS) of these misfit layer compounds [18], where the first 3d t_{2g}-type peak of the XAS spectra of $(SbS)_{1.15}TiS_2$ shifted about 0.17 eV to higher energy, in comparison with $(SbS)_{1.15}(TiS_2)_2$.

The Hall coefficient, R_H (figure 3), for the two misfit layer compounds is negative and independent of magnetic field up to 3.0 T in the temperature range of 4.2–300 K, indicating only one type of charge carrier. As the temperature increases, the Hall coefficient R_H for the stage-2 compound decreases and attains a constant value above 100 K; however, R_H for the stage-1 compound first decreases with increasing temperature and then increases and reaches a constant value above about 200 K. A minimum occurs at about 80 K. In contrast, a maximum in R_H as a function of temperature has been found for the intercalates Li_xTiS_2 with high carrier concentration as well as for self-intercalated $Ti_{1+x}S_2$ with $x = 0.014$ [27]. Assuming that a single-carrier model is valid here, the electron concentration n can be evaluated from the simple relation $n_e = -1/eR_H$. At $T = 4.2$ K the electron concentration calculated in this way is 5.0×10^{27} m^{-3} for the stage-1 compound, corresponding to 0.57 electrons per Ti atom; and is 4.0×10^{27} m^{-3} for the stage-2 compound, corresponding to 0.34 electrons/Ti. Assuming electron donation from the SbS layers to the TiS_2 sandwiches, $0.57/1.15 = 0.5$ electron/Sb is transferred in the stage-1 misfit layer compound; and the slightly larger electron donation ($2 \times 0.34/1.15 = 0.59$ electron/Sb) in the stage-2 compound is due to some self-intercalated Ti atoms in the *empty* van der Waals gaps. The content of intercalated Ti atoms is estimated to be about 0.02 per formula unit cell.

The temperature dependence of the thermopower, S, for the two misfit layer compounds, is plotted in figure 4. The negative value of S over the temperature range 4.2–300 K indicates that the conduction carriers are electrons. The absolute value of S at room temperature for the stage-1 compound is smaller than for the stage-2 compound, which indicates that the number of electrons per Ti in the stage-1 compound is larger than in the stage-2 compound, in agreement with the Hall effect. The non-linear temperature dependence of the thermopower for 1T-TiS_2

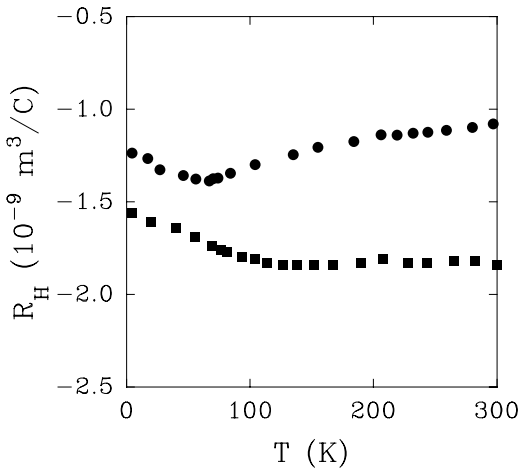

Figure 3. The temperature dependence of the Hall coefficient R_H of $(SbS)_{1.15}TiS_2$ (filled circles) and that of $(SbS)_{1.15}(TiS_2)_2$ (filled squares).

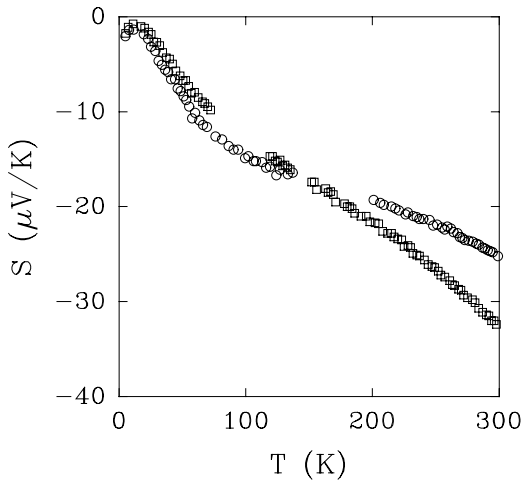

Figure 4. The temperature dependence of the thermopower S of $(SbS)_{1.15}TiS_2$ (open circles) and that of $(SbS)_{1.15}(TiS_2)_2$ (open squares).

and its intercalates $\mathcal{M}'_xTiS_2$ ($\mathcal{M}'$ = Mo, Fe, Co and Ni) has been analysed by Koyano *et al* [8], on the basis of the model of Klipstein *et al* [13]. However, attempts to use their model to fit the thermopower of these misfit layer compounds failed.

4. Optical properties

4.1. Reflectance spectra

The room temperature reflectivities of the Sb misfit layer compounds are shown in figure 5. Each spectrum shows a well-defined plasma edge at low photon energies. In the energy region higher than the plasma edge the spectra of the layer compounds reveal a shoulder around $\omega = 10\,000\ cm^{-1}$. Above $\omega = 10\,000\ cm^{-1}$ the reflectivities of both misfit layer compounds

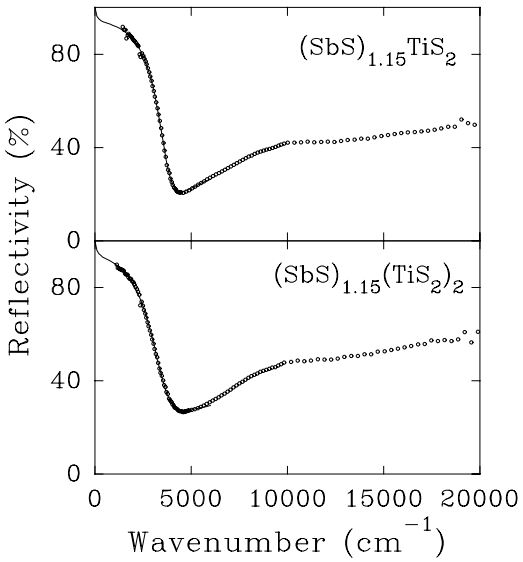

Figure 5. Reflectivities for $(SbS)_{1.15}TiS_2$ and $(SbS)_{1.15}(TiS_2)_2$. The circles and squares show measured data and solid curves are calculated from fit parameters (see table 4).

continue to increase, indicating another peak at higher energies, which might be due to the interband transitions in the SbS subsystem.

In the first step we have analysed the spectra in the low-energy region with a single-carrier Drude model for the free electron system. The reflectivity is written as

$$R = \frac{(N-1)^2 + K^2}{(N+1)^2 + K^2}, \tag{2}$$

where the real refractive index N and the attenuation index (extinction coefficient) K are expressed as

$$\begin{aligned} N &= \sqrt{\tfrac{1}{2}\left[\sqrt{\epsilon_1^2 + \epsilon_2^2} + \epsilon_1\right]}, \\ K &= \sqrt{\tfrac{1}{2}\left[\sqrt{\epsilon_1^2 + \epsilon_2^2} - \epsilon_1\right]}, \end{aligned} \tag{3}$$

with the real and imaginary parts of the dynamic dielectric function

$$\begin{aligned} \epsilon_1(\omega) &= \epsilon_\infty\left(1 - \frac{\omega_p^2}{\omega^2 + \Gamma^2}\right), \\ \epsilon_2(\omega) &= \frac{\epsilon_\infty \omega_p^2 \Gamma}{\omega(\omega^2 + \Gamma^2)}, \end{aligned} \tag{4}$$

where ω_p is the screened plasma frequency, Γ the frequency-independent damping constant, ϵ_∞ the high-frequency dielectric constant and ω the angular frequency.

The three parameters (ϵ_∞, ω_p and Γ) were used for non-linear least-squares fits to the experimental data. However, fits to the spectra of the misfit layer compounds completely failed. Considering a possible experimental error (5%), attempts to perform Drude fits to the modified data, multiplied by a factor of 0.95 and 1.05, failed as well. This unsatisfactory results could be due to the interband absorption in the Drude regions. It is known that the energy gap between the S 3p valence band and Ti 3d conduction band in 1T-TiS_2 can be as

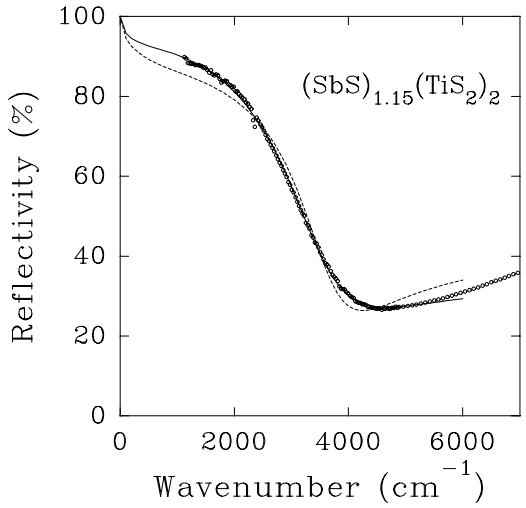

Figure 6. The reflectivity of $(SbS)_{1.15}(TiS_2)_2$. The filled circles represent the measured data; the dashed curve is the best fit using the Drude model for a Fermi gas, while the solid curve is the fit using the Fermi-liquid model.

Table 4. Optical parameters derived from the room temperature reflectivity of $Ag_{0.20}TiS_2$, $Ag_{0.36}TiS_2$ and $(SbS)_{1.15}(TiS_2)_n$ $(n = 1, 2)$.

Compound	ω_p (cm^{-1})	ϵ_∞	Γ_0 (cm^{-1})	p (cm^{-1} K^{-1})
$(SbS)_{1.15}TiS_2$	4015	14.5	529	9.7
$(SbS)_{1.15}(TiS_2)_2$	4150	14.4	647	7.5

small as 0.1 eV. Thus the interband transitions of S 3p $\rightarrow$ Ti 3d will begin at low energy, perhaps with a maximum at 10 000 cm^{-1}. Even so, the SbS subsystem of the misfit layer compounds could reveal an interband transition which may well extend to frequencies below ω_p. Another possible explanation of the deviation is related to a frequency dependence of the scattering rate, as pointed out by Julien *et al* [14] in a study of the optical reflectivity of TiS_2. A satisfactory fit to the optical data for the misfit layer compounds was achieved by using the Fermi-liquid model with a frequency-dependent scattering rate (the inverse relaxation time):

$$\frac{1}{\tau_{ee}(T,\omega)} = \Gamma(T,\omega) = \Gamma_0(T)\left[1 + \left(\frac{\omega}{pT}\right)^2\right], \tag{5}$$

where $\Gamma_0(T) = 1/\tau_{0,ee}(T)$ is a temperature-dependent parameter, p a constant and T is taken to be 300 K (room temperature). Figure 6 illustrates the difference in the fits to the reflectivity data of $(SbS)_{1.15}(TiS_2)_2$ using the frequency-independent damping constant Γ (the dashed curve) and the frequency-dependent scattering rate (equation (5)) (the solid curve). The values of the fit parameters (ω_p, ϵ_∞, Γ_0 and p) are given in table 4. Observed and calculated spectra for the samples are shown as the solid curves in figure 5. For both misfit layer compounds, the parameter p is larger than the value $p = 2\pi$ which is expected for ideal Fermi-liquid behaviour in the isotropic three-dimensional effective mass model [28]. Julien *et al* [14] have found, for the optical reflectivity of 1T-TiS_2, $p \approx 4\pi$ instead of $p = 2\pi$. The high values of p for these misfit layer compounds may be related to this layered structure.

It is worth pointing out that the Drude and Fermi-liquid models have only been fitted to the data from the low-frequency limit to slightly above the reflectivity minimum at ω_0 (up

to $\omega = 6000\ \mathrm{cm}^{-1}$). Hence the fit is governed by ω_0 and the line shape below ω_0. Further extension to higher wavenumber of the data for the fit substantially reduces the quality of the fit below ω_0. This shows that for the spectra above $\omega = 6000\ \mathrm{cm}^{-1}$ the influence of additional absorption becomes important.

4.2. Anisotropy

The in-plane anisotropy of the misfit layer compound $(SbS)_{1.15}TiS_2$ has been investigated by measuring the reflectivity of a thinned sample in the region $\omega = 3000$–$9400\ \mathrm{cm}^{-1}$ using polarized incident light. Figure 7 shows the reflectivities of a thin sample at various angles Θ between the electrical field vector of the polarized incident light and a direction in the ab-plane. The wavy curves between $\omega = 5000$ and $8000\ \mathrm{cm}^{-1}$ are due to interference of the light in the thin specimen. A small but significant Θ-dependent change of the spectra is observed. This is more clearly demonstrated in figure 8, where the variation of the reflectivity at $\omega = 3500\ \mathrm{cm}^{-1}$ (filled squares) and the frequency ω_0 (filled circles), the frequency of the minimal reflectivity, are shown as a function of the angle Θ. The angle-dependent variation of the reflectivity showed the relation

$$R(\Theta) = R_0 \cos^2(\Theta - \Theta_0) + R_{\pi/2} \sin^2(\Theta - \Theta_0), \tag{6}$$

revealing an in-plane anisotropy. A least-squares fit obtains $\Theta_0 = 28.5°$, $R_0 = 0.384$ and $R_{\pi/2} = 0.366$. With the same argument as above, the angle dependence of ω_0 can be expressed as

$$\omega_0(\Theta) = \omega_0(0) \cos^2(\Theta - \Theta_0') + \omega_0(\pi/2) \sin^2(\Theta - \Theta_0'), \tag{7}$$

with $\Theta_0' = 31.0°$, $\omega_0(0) = 4487\ \mathrm{cm}^{-1}$ and $\omega_0(\pi/2) = 4656\ \mathrm{cm}^{-1}$. Thus, small shifts in ω_0 and in the absolute value of reflectivity are observed. A similar effect has also been reported for the misfit layer compound $(PbS)_{1.11}TaS_2$ [4], which was explained by an effect in the effective masses of the free carrier system for $\vec{E} \parallel \vec{a}^*$ with respect to $\vec{E} \parallel \vec{b}^*$. In further studies concerning this effect on many other misfit layer compounds, it was found that the free carrier reflectivity behaviour always implies systematically somewhat smaller ω_p-values (by about 1–5%) for the electrical field polarized parallel to the incommensurate lattice direction [29]. Thus, a similar explanation may be applied to the ab-plane anisotropy observed for $(SbS)_{1.15}(TiS_2)_n$ with $n = 1, 2$.

5. Discussion

In a simple metal such as gold, the relaxation time τ_{ee} due to electron–electron interactions is of the order of $\tau_{ee} \sim 10^{-11}$ s [30], which is much longer than the relaxation time $\tau_{ep} \sim 10^{-14}$ s [31] due to electron–phonon scattering. Therefore, electron–electron scattering has a negligible effect on the dc conductivity of normal metals. From the fit parameter for the optical spectra of the misfit layer compounds, we find the relaxation time $\tau_{0,ee} \sim 0.5 \times 10^{-13}$ s at room temperature, which is close to τ_{ep}. According to equation (5), $\tau_{ee}(T, \omega)$ decreases rapidly with increasing frequency.

It is useful to compare the optical properties with the electrical transport properties. In combination with the results for the electrical resistivity and the optical reflectivity, the relaxation time may be written as

$$\frac{1}{\tau(T, \omega)} = \beta[(pT)^2 + \omega^2] \ln \frac{T_F}{T}, \tag{8}$$

where β and p are constants, and T_F the Fermi temperature.

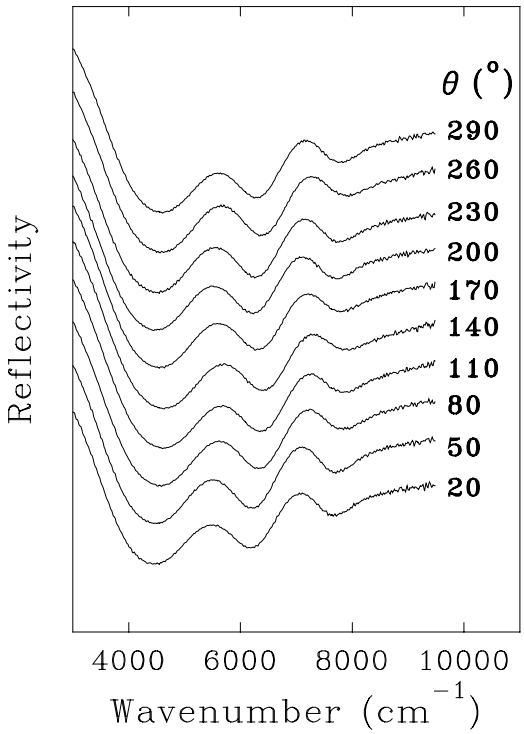

Figure 7. The reflectivity of $(SbS)_{1.15}TiS_2$ at different angles Θ between the electrical field vector of the polarized incident light and a direction in the *ab*-plane.

From the carrier concentration n_e obtained from the Hall measurements, the optical effective mass m_{opt} can be derived from the following equation:

$$\omega_p^2 = \frac{n_e e^2}{\epsilon_0 \epsilon_\infty m_{opt}}, \tag{9}$$

where $\epsilon_0 = 8.85 \times 10^{-12}$ A s V^{-1} m^{-1}, n_e is the free carrier concentration, m_{opt} the optical mass. We calculated the optical effective masses to be 1.9 and 1.4 m_e (where m_e is the electron rest mass and the carrier concentrations as obtained from the Hall effect measurements at 4.2 K are used here) for $(SbS)_{1.15}TiS_2$ and $(SbS)_{1.15}(TiS_2)_2$, respectively. Logothetis *et al* [32] observed a difference between the value of the free carrier concentration calculated from Hall effect measurements (n_{Hall}) and the optical studies (n_{opt}) for various degrees of non-stoichiometry x of $Ti_{1+x}S_2$. They found that the ratio between n_{opt} and n_{Hall} is a constant of 1.3 for all the samples. On the other hand, because of the interaction of the conduction electrons with each other through their electrostatic interaction, the electrons suffer collisions. A moving electron causes an inertial reaction in the surrounding electrons, thereby increasing the effective mass of the electron. Using the Fermi energies (table 4) obtained from the fits to the resistivities, together with the relaxation times obtained from the optical spectra, the mean free paths l for electron–electron collisions at room temperature and $\omega = 0$ can be estimated to be $l_{ee} = v\tau = \sqrt{2E_F/m^*}\tau \approx 10^{-7}$ cm, which is even smaller than that ($l_{ep} \approx 10^{-6}$ cm [31]) for electron–phonon scattering.

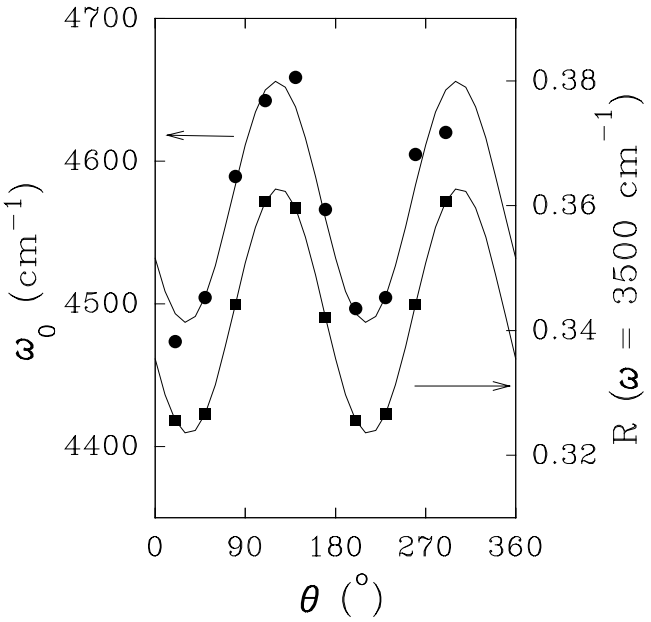

Figure 8. Variations of the frequency ω_0 and the reflectivity R at $\omega = 3500$ cm^{-1} as a function of the angle Θ for $(SbS)_{1.15}TiS_2$ (see figure 7).

Within the Drude model the optical dc conductivity σ_{opt} can be expressed as

$$\sigma_{opt} = \frac{\omega}{4\pi}\epsilon_2 = \frac{\epsilon_0\epsilon_\infty\Gamma\omega_p^2}{\omega^2 + \Gamma^2}. \tag{10}$$

We obtained room temperature optical resistivities at $\omega = 0$ as $\rho_{opt} = 1/\sigma_{opt} = 1.4 \times 10^{-6}$ and 1.6×10^{-6} Ω m for the stage-1 and the stage-2 misfit layer compounds, respectively. These values are larger than the in-plane electrical resistivities at room temperature, which are 0.7×10^{-6} and 1.5×10^{-6} Ω m for the stage-1 and stage-2 compounds, respectively. This is consistent with the experimental result for Fermi-liquid systems that the resistivity of the sample deduced from the optical measurements is always larger than the same quantity measured with a dc current (pp 109–110 of [30]). It is generally found that the scattering rate $(1/\tau)$ has a quadratic variation with frequency, as for quasiparticles in 3D Fermi-liquid systems.

6. Conclusions

The electrical transport and optical properties of stage-1 and stage-2 misfit layer compounds $(SbS)_{1.15}(TiS_2)_n$ with $n = 1, 2$ were studied. Near-infrared reflectivity and Hall effect measurements consistently show a large number of doped electrons per Ti atom from the compound with $n = 1$. The in-ab-plane electrical resistivities exhibit a non-linear dependence on temperature, which is closely related to the similar behaviour observed for 1T-TiS_2 and its intercalates. This also indicates that the TiS_2 subsystem dominates the electrical transport mechanism. The variation of the in-plane resistivity follows well the expected behaviour of a 2D Fermi liquid (equation (1)). The Fermi energies deduced, $E_F = k_B T_F$, are 0.29 eV for $(SbS)_{1.15}TiS_2$ and 0.16 eV for $(SbS)_{1.15}(TiS_2)_2$, indicating a higher filling level of the

conduction band of the stage-1 compound. The dominance of electron–electron scattering, which is indicative of a Fermi-liquid property, is also inferred from the optical reflectivity data where a quadratic frequency dependence of the relaxation time of the free carrier system is observed. A small anisotropy in the ab-plane is visible in the reflectivity spectra using polarized light.

Acknowledgments

We are very grateful to Mr J Baas for assistance with electrical transport measurements. The optical measurements were carried out at the Department of Mineralogy at the University of Hannover, Germany. This work is part of the research programme of the Stiching voor Scheikundig Onderzoek Nederland (SON), which is financially supported by the Nederlandse Organisatie voor Wetenschappelijk Onderzoek (NWO).

References

[1] Wiegers G A and Meerschaut A 1992 Incommensurate sandwiched layered compounds *Material Science Forum* vols 100 and 101, ed A Meerschaut (New York: Trans. Tech.) p 101
[2] Wiegers G A 1996 *Solid State Chem.* **1–2** 1
[3] van Smaalen S 1992 Incommensurate sandwiched layered compounds *Material Science Forum* vols 100 and 101, ed A Meerschaut (New York: Trans. Tech.) p 173
[4] Rüscher C H, Haas C, van Smaalen S and Wiegers G A 1994 *J. Phys.: Condens. Matter* **6** 2117
[5] Berner D, Leihenseder H, Widder K, Geserich H P, Burlakov V M, Mavrin B N, Denisov V N, Roesky R, Gressier P and Meerschaut A 1997 *J. Phys.: Condens. Matter* **9** 10 545
[6] Gerards A G, Roede H, Haange R J, Bukamp B A and Wiegers G A 1984/85 *Synth. Met.* **10** 51
[7] Friend R H and Yoffe A D 1987 *Adv. Phys.* **36** 1
[8] Koyano M, Negishi H, Ueda Y, Sasaki M and Inoue M 1986 *Phys. Status Solidi* b **138** 357
[9] Ueda Y, Negishi H, Koyano M, Inoue M, Soda K, Sakamoto H and Suga S 1986 *Solid State Commun.* **57** 839
[10] Kukkonen C A, Kaiser W J, Logothetis E M, Blumenstock B J, Schroeder P A, Faile S P C and Gambold J 1981 *Phys. Rev.* B **24** 1691
[11] Wilson J A 1978 *Phys. Status Solidi* b **86** 11
[12] Inoue M, Hughes H P and Yoffe A D 1989 *Adv. Phys.* **38** 565
[13] Klipstein P C, Bagnall A G, Liang W Y, Marseglia E A and Friend R H 1981 *J. Phys. C: Solid State Phys.* **14** 4067
[14] Julien C, Ruvalds J, Virosztek A and Gorochov O 1991 *Solid State Commun.* **79** 875
[15] Wiegers G A and Haange R J 1991 *Eur. J. Solid State Inorg. Chem.* **28** 1071
[16] Ren Y, Meetsma A, Petricek V, van Smaalen S and Wiegers G A 1995 *Acta Crystallogr.* B **51** 275
[17] Ren Y, Meetsma A, Wiegers G A and van Smaalen S 1995 *Acta Crystallogr.* B **52** 389
[18] Ren Y, Haas C and Wiegers G A 1995 *J. Phys.: Condens. Matter* **7** 1
[19] Klipstein P C and Friend R H 1987 *J. Phys. C: Solid State Phys.* **20** 4169
[20] Meakin J I, Klipstein P C and Friend R H 1987 *J. Phys. C: Solid State Phys.* **20** 271
[21] Thompson A H 1975 *Phys. Rev. Lett.* **35** 1786
[22] Takagi H, Batlogg B, Kao H L, Kmo J, Cava R J, Krajewski J J and Peck W F Jr 1992 *Phys. Rev. Lett.* **69** 2975
[23] Brinkmann M, Rex T, Bach H and Westerholt K 1995 *Phys. Rev. Lett.* **74** 4927
[24] Tsuei C C, Gupta A and Koren G 1989 *Physica* C **161** 415
[25] Hodges C, Smith H and Wilkins J W 1971 *Phys. Rev.* B **4** 302
[26] Giuliani G F and Quinn J J 1982 *Phys. Rev.* B **26** 4421
[27] Inoue M, Koyano M, Negishi H, Ueda Y and Sato H 1985 *Phys. Status Solidi* b **132** 295–303
[28] Gurzhi R N 1959 *Sov. Phys.–JETP* **35** 673–5
[29] Rüscher C H, Haas C and Wiegers G A 1996 unpublished
[30] Abelès F 1972 *Optical Properties of Solids* (Amsterdam: North-Holland)
[31] Haug A 1972 *Theoretical Solid State Physics* vol 2 (Oxford: Pergamon)
[32] Logothetis E M, Kaiser W J, Kukkonen C A, Faile S P, Colella R and Gambold J 1980 *Physica* B **99** 193